The k-trajectory formulation of the NMR imaging process with applications in analysis and synthesis of imaging methods

Donald B. Twieg

Department of Radiology, The University of Texas Health Science Center at Dallas, Dallas, Texas 75235

(Received 1 October 1982; accepted for publication 5 April 1983)

The fundamental operations of nuclear magnetic resonance (NMR) imaging can be formulated, for a large number of methods, as sampling the object distribution in the Fourier spatial-frequency domain, followed by processing the digitized data (often simply by Fourier transformation) to produce a digital image. In these methods, which include reconstruction from projections, Fourier imaging, spin-warp imaging, and echo-planar imaging, controllable gradient fields determine the points in the spatial-frequency domain which are sampled at any given time during the acquisition of data (the free induction decay, or FID). The detailed time dependence of the resulting trajectory of sample points (the k trajectory) determines the relative weight and accuracy with which image information at each spatial frequency is measured, establishing theoretical limitations on image quality achievable with a given imaging method. We demonstrate here that these considerations may be used to compare the theoretical capabilities of NMR imaging methods, and to derive new imaging methods with optimal theoretical imaging properties.

I. INTRODUCTION

A nuclear magnetic resonance (NMR) imaging instrument forms images by causing the object being imaged to emit radio-frequency signals which contain information. That information concerns the spatial distribution of nuclear magnetization within the object. (More precisely, it concerns the magnitude of the transverse component of the magnetization, which in general reflects spin density and the relaxation times T_1 and T_2 in combination. Although rf pulse sequences may be applied which cause the image to reflect predominantly one of these quantities alone, in all cases the transverse component of the magnetization is the quantity whose distribution is represented in the radio-frequency signal.) Various techniques have been devised to encode this basic information into the radio-frequency signal by means of rf pulses and time-varying gradient fields.

Just as each NMR imaging method has a strategy for encoding spatial information into a noisy NMR signal, each method must have a corresponding decoding procedure, which extracts the desired information from the noisy signal. Often any one of a number of different decoding procedures can be used with a given encoding procedure. As in the case of the computational procedures used for reconstructing images from CT (computerized tomography) projections, some decoding procedures are more accurate, more reliable, or more efficient than others, but in all cases the information in the final image can be no better than the information present in the noisy data. Thus the process of encoding spatial information is worth some scrutiny, as it is a major determinant of the quality of information in the displayed NMR image.

Other imaging modalities, such as CT imaging, offer limited opportunity for improving image quality by improving the encoding process, since encoding can only be done in a rather limited number of ways. In contrast, there are a very large number of potentially workable NMR imaging methods, and the quality of the encoding operation, and hence the quality of images available, varies a great deal among them.

The aim of this communication is to present a new approach to understanding the encoding process in NMR imaging, and to present a few of the applications of this approach in performance analysis of NMR imaging methods, and in synthesis of new NMR imaging methods.

Encoding in NMR imaging has been understood as a process of producing NMR spectra corresponding directly to spatial projections largely because NMR imaging developed largely as an extension of NMR spectroscopic methods.

Unfortunately, there are some significant disadvantages to this approach—it obscures some fundamental similarities between various existing methods, and it fails to provide a consistent and convenient theoretical framework for quantitatively assessing imaging performance.

An alternative and equally valid viewpoint exists, however, which provides both a useful intuitive picture of the imaging process and an analytic model which allows consistent comparison of imaging performance for existing methods and derivation of new imaging methods with desired performance characteristics.

This alternative viewpoint, which we call for convenience the k-trajectory formulation, has been noted before.[1] Its application as an analytic model for assessing imaging performance, and its potential in deriving improved NMR imaging techniques, have been remarked only recently,[2] and are discussed in detail for the first time in this communication.

The essence of the k-trajectory formulation is that time-varying gradients map the spatial-frequency-domain content of the object directly into the FID signal. As will be shown in Sec. II A, this mapping may be visualized in terms of a trajectory in the spatial-frequency domain (or k domain) referred to as a k trajectory.

The k-trajectory formulation applies only to those methods in which an FID (with or without "echoes") is produced.

 0094-2405/83/050610-12$01.20

Methods which use steady-state free precession as the excitation mechanism[3,4] cannot be formulated readily in k-trajectory terms.

We refer to the large class of methods describable in k-trajectory terms as the generalized Fourier NMR imaging methods, because of the fundamental Fourier transform relationship between the data (the FID) and the image. The term "generalized" is used because these methods map the spatial-frequency (Fourier) domain information into the FID, but in general they do not perform this mapping linearly, as do existing techniques with constant encoding gradients.

Among the generalized Fourier NMR imaging methods are most established imaging methods: The original Fourier method of Kumar, Welti, and Ernst[5]; the spin-warp method of Edelstein *et al.*[6]; the zeugmatographic or reconstruction from projections method of Lauterbur and colleagues[7–9]; the echo-planar method of Mansfield and colleagues[10–12]; the rotating frame method of Hoult[13]; modifications of these methods.[14–16]

The list of potentially workable generalized Fourier methods could go on indefinitely; there are an infinite number of ways to scan the k domain which will successfully place into the FIDs sufficient information to permit image formation from the FIDs. Each of these encoding schemes will have advantages and disadvantages in terms of the quality of image information it conveys, and in terms of the ease of implementation of its gradient program, and its sampling and decoding (computational) procedures. Some of these unrealized methods appear to offer significant performance advantages.

In tomographic NMR imaging, images representing two-dimensional "slices" of an object are produced. The following development applies to generalized Fourier NMR methods regardless of the means they use for slice selection. Methods using Fourier slice selection[17] (which is equivalent to the three-dimensional Fourier method), selective excitation,[7,18] and oscillating gradients[19] may all be treated by the k-trajectory formulation. When oscillating gradients are used, signal averaging over periods long with respect to the period of oscillation greatly attenuates the net signal contribution from spins outside the region of constant field.

II. THE GENERAL k-TRAJECTORY VIEW OF NMR IMAGING

A. k trajectories

In the imaging methods with which we are concerned, a complex signal $s(t)$ (known as a **free induction decay** or FID in Fourier NMR spectroscopy[20,21]) is evoked from a spin system in response to an applied radio-frequency pulse. Suppose a homogeneous static magnetic field **Ho** is imposed on an object with magnetization distribution $f(\mathbf{x})$ where $\mathbf{x}$ is a two- or three-dimensional set of spatial coordinates in vector form. The spins in the object are assumed to have the same gyromagnetic ratio[21,22] γ throughout, and the FID is assumed to be the result of quadrature phase detection referred to the common Larmor frequency.

If the exciting rf pulse is applied with center at time $t = 0$, the complex FID following the rf pulse will be (for $t > 0$):

$$s(t) = \int_V \exp(-t/T_2) f(x) \exp[-i2\pi \mathbf{k}(t) \cdot \mathbf{x}]\, d\mathbf{x}, \qquad (1)$$

where T_2 is the spin–spin relaxation time.[22] Here $\mathbf{k}(t)$ is defined as

$$\mathbf{k}(t) = \gamma \int_0^t dH(t')/d\mathbf{x}\, dt', \qquad (2)$$

where γ is the nuclear gyromagnetic ratio for the nucleus being imaged.

The vector quantity $\mathbf{k}(t)$ is the integral of the gradients, but it can also be seen in Eq. (1) as the vector of spatial-frequency coordinates. That is, Eq. (1) can be rewritten as

$$s(t) = \exp(-t/T_2) F[\mathbf{k}(t)], \qquad (3)$$

where for simplicity, we assume T_2 to have only one value within the object, and where F is the Fourier transform of the object spatial distribution $f(\mathbf{x})$.

It is not necessary to assume that the FID results from perturbation of the spin systems by a single rf pulse. Any of the multiple-pulse methods[21,22] for determining spin–spin and spin-lattice relaxation times T_1 and T_2, for instance, may be treated in their adapted imaging forms[6] by essentially the same model developed below.

Equation (3) suggests that we can see the continuous-time FID, $s(t)$, as a weighted (and noisy) observation of the spatial frequency distribution $F(\mathbf{k})$ corresponding to the original object. The encoding process, then, consists of sampling along a set of k trajectories determined by the time-varying gradients, and the decoding process consists of processing those samples (usually by means of the Fourier transform) to obtain a discrete image which is an estimate of the original spatial distribution. The remainder of this communication will examine the details of these encoding and decoding processes, and how the choice of imaging method thereby influences imaging performance.

B. Sampling and discretization

In practice, NMR images are invariably displayed digitally, so the final image is a function of a discrete variable, as is the original data—the sampled and digitized FID—used to generate the image. It seems appropriate, then, to consider the operation of the encoding and decoding processes in the discrete-variable form in which they actually occur after sampling.

In many imaging methods, the sampling process itself occurs in essentially the same way—each discrete sampled value corresponds to integration with an identical sampling kernel at a rectangular grid point in k space. Thus for purposes of comparing relative performance among these methods, only the discrete postsampling encoding and decoding procedures involving discrete variables need be considered.

Consider an imaging method which uses a set of FIDs identified by the index $j = 0,1,2,\ldots,J-1$, and suppose each is distinct. In other words, for the time being, we assume (with no loss of generality) that all k locations sampled are sampled only once, and ignore signal averaging in which a k location is sampled multiple times by repeated k trajectories.

Suppose the FID $s_j(t)$ is periodically sampled throughout

the course of the FID at times t_{jp} ($p = 0,1,2,...,N-1$), and suppose that the pth sample represents an integration of $s_j(t)$ over the interval $[t_{jp}, t_{jp} + \Delta t_{jp}]$, where

$$\Delta t_{jp} \leqslant (t_{jp+1} - t_{jp})$$

(Fig. 1). Denote the resulting sequence of N values as s_{jp}:

$$s_{jp} = \int_{t_{jp}}^{t_{jp}+\Delta t_{jp}} \exp(-t/T_2)\, F[\mathbf{k}_j(t)]\, dt. \tag{4}$$

If neither of the integrand factors changes substantially over the interval of integration, we may write the approximate expression

$$s_{jp} = \Delta t_{jp} \exp(-t_{jp}/T_2)\, F[\mathbf{k}_j(t_{jp})], \tag{5}$$

with $j = 0,1,...,(J-1)$ and $p = 0,1,...,(N-1)$. Neglecting noise considerations, then, the complete set of FID data represented by the two-dimensional $N \times J$ array $\{s_{jp}\}$ is a set of weighted samples of the image k-domain distribution $F[\mathbf{k}_j(t_{jp})]$.

If the sample k values [specified by the k trajectories $\mathbf{k}_j(t)$ and the sample time and interval sequences t_{jp} and Δt_{jp}] are arranged on a rectangular grid in the k domain, we can simply treat the data values as a discrete Fourier-domain image, and obtain our discrete spatial-domain image by applying a two- or three-dimensional discrete Fourier transform. Most of the established NMR imaging methods operate in this fashion. For purposes of comparing methods which sample on a rectangular grid, the approximation errors in Eq. (5) are irrelevant, since they are the same for each of those methods.

For some of the established methods (reconstruction from projections and the echo-planar methods), and for the general case, however, the samples are not taken on a rectangular grid. In these cases, in order to apply the discrete Fourier transform to obtain a discrete image array for display, a rectangular array of k samples may be computed (interpolated) from the irregularly spaced sample array.

The reconstruction from projections method most often uses a filtered backprojection or similar reconstruction algorithm rather than interpolation and Fourier inversion, though the latter process can be used. For our purposes, it is useful to consider the reconstruction from projections methods as operating in this sampling–interpolation–inverse transform sequence, just as the other generalized Fourier methods do.

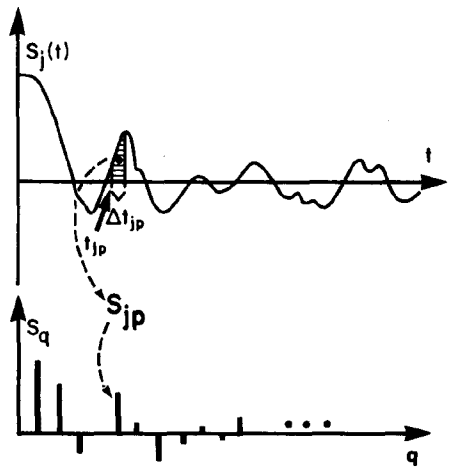

FIG. 1. The datum s_{jp} results from sampling the jth FID $s_j(t)$ during the pth time interval $[t_{jp}, t_{jp} + \Delta t_{jp}]$, and corresponds to a datum s_q in the discrete spatial-frequency coordinate q.

The NJ data values of Eq. (5) could represent data from either two- or three-dimensional Fourier imaging procedures. In the case of the spin-warp method, or the original Fourier method in their three-dimensional implementations, if a cubic array of image elements ($N \times N \times N$) were to be formed, N^2 FIDs could be used, so that $J = N^2$.

Let $\mathbf{q}$ be the vector of discrete spatial frequency indices. Then the data s_{jp} can be rearranged into a discrete spatial-frequency array $s_\mathbf{q}$ such that the inverse discrete Fourier transform (DFT) will produce from it an estimated image $f_d(\mathbf{n})$, where $\mathbf{n}$ is a vector of spatial coordinate indices. Suppose the sample times t_{jp} are reordered into the array $t_\mathbf{q}$, as was the sample array s_{jp}. The data are then given by

$$s_\mathbf{q} = \Delta t_\mathbf{q} \exp(-t_\mathbf{q}/T_2)\, F[\mathbf{k}_\mathbf{q}], \tag{6}$$

where $\mathbf{k}_\mathbf{q}$ is the k-sampling point corresponding to the discrete spatial-frequency index $\mathbf{q}$.

As we have seen, the encoding procedure which characterizes a given generalized Fourier method is defined by (1) its set of k trajectories $\{\mathbf{k}_j(t),\ j = 0,1,2,...,J-1\}$, and (2) its schedule of FID sampling times t_{jp} or periods Δt_{jp}, $j = 0,1,...,J-1$; $p = 0,1,...,N-1$.

There is a set of basic sampling requirements for image formation associated with an object's size and the dimension of the desired image array. Specifically, two basic requirements must be satisfied by any method. These are (1) the range of sampling within the k domain must include all spatial frequencies present in significant amount within the object and (2) the frequency of sampling within the k domain must, on the average, match the extent of the object (i.e., $\Delta k = K/N \leqslant 1/X$).

The second requirement seems to allow arbitrary sampling density locally, so long as the net sampling density is adequate. However, there are practical restrictions on how sparsely one may sample locally, which are determined in part by the noise content of the data.[23,24]

C. Statistical characteristics of NMR imaging data

The function $F(\mathbf{k})$, via the sampling process, determines the value of the idealized discrete spatial frequency function $F_d(\mathbf{q})$. Since the datum $s_\mathbf{q}$ is the observed value for this function, and $s_\mathbf{q}$ is implicitly interpreted by many established methods as $F_d(\mathbf{q})$, we define the observed distribution $F_0(\mathbf{q}) = As_\mathbf{q}$, where A is a scalar constant. If we include random noise as an additive term $V'(\mathbf{q})$, we have the linear discrete observation equation

$$F_0(\mathbf{q}) = H(\mathbf{q})\, F_d(\mathbf{q}) + V'(\mathbf{q}), \tag{7}$$

for all $\mathbf{q}$, where

$$H(\mathbf{q}) = A\Delta t_\mathbf{q} \exp(-t_\mathbf{q}/T_2). \tag{8}$$

The noise $V'(\mathbf{q})$ will be assumed to have zero mean and variance $E\{|V'(\mathbf{q})|^2\}$ proportional to $\Delta t_\mathbf{q}$, and to be independent of the object distribution. This last assumption seems justified under most expected NMR imaging circumstances.[25]

Suppose we choose to represent the distribution $f(\mathbf{x})$ by a

digital image which is just the inverse transform of F_0. In other words, we simply perform the inverse transform and do not process the data in any other way. Then the quality of the image representation as measured in the spatial-frequency domain could be judged on the basis of the error in $F_0(\mathbf{q})$ as an estimate of $F_d(\mathbf{q})$. This error is a random number, with mean

$$E\{F_d(\mathbf{q}) - F_0(\mathbf{q})\} = [1 - H(\mathbf{q})]\, F_d(\mathbf{q}), \tag{9}$$

and expected square error

$$E\{|F_d(\mathbf{q}) - F_0(\mathbf{q})|^2\}$$

$$= |[1 - H(\mathbf{q})]\, F_d(\mathbf{q})|^2 + \mathrm{var}\{V'(q)\}, \tag{10}$$

where $E\{\ \}$ denotes the expected value of the bracketed quantity.

Generally, some postacquisition processing will be used, such as simple two-dimensional low-pass filtering of the image, or application of a "matched" filter[20] to the FID. In most cases, this processing may be modeled as a linear shift-invariant operation, corresponding to discrete convolution with a fixed kernel in the spatial domain, or to multiplication by a discrete filter transfer function in the spatial-frequency domain.[26,27]

If the resulting spatial-frequency estimate is $F_e(\mathbf{q})$, and the linear filter is $H_r(\mathbf{q})$, then

$$F_e(\mathbf{q}) = H_r(\mathbf{q})\, F_0(\mathbf{q}) = H_r(\mathbf{q})\, \{H(\mathbf{q})\, F_d(\mathbf{q}) + V'(\mathbf{q})\}. \tag{11}$$

In this case the mean of the estimate error

$$F_{\mathrm{err}}(\mathbf{q}) = F_d(\mathbf{q}) - F_e(\mathbf{q})$$

is

$$E\{F_{\mathrm{err}}(\mathbf{q})\} = [1 - H_r(\mathbf{q})\, H(\mathbf{q})]\, F_d(\mathbf{q}), \tag{12}$$

and the expected square estimate error is

$$E\{|F_{\mathrm{err}}(\mathbf{q})|^2\} = |[1 - H_r(\mathbf{q})\, H(\mathbf{q})]\, F_d(\mathbf{q})|^2 + |H_r(\mathbf{q})|^2\, \mathrm{var}\{V'(\mathbf{q})\}, \tag{13}$$

where $V'(\mathbf{q})$ is uncorrelated with the image distribution. For unbiased methods, in which $H_r(\mathbf{q}) = H(\mathbf{q})^{-1}$, the first term on the right-hand side of Eq. (13) vanishes, and the expected square estimate error becomes the estimate error variance $V_{\mathrm{es}}(\mathbf{q})$.

Equation (13) represents really a special case; in general, there may be correlation between the measurement errors $F_{\mathrm{err}}(\mathbf{q})$ and $F_{\mathrm{err}}(\mathbf{q}')$ so that error variance can be completely expressed only in terms of a covariance matrix with the $(\mathbf{q},\mathbf{q}')$th element given by

$$P_{\mathrm{err}}(\mathbf{q},\mathbf{q}') = E\{F^*_{\mathrm{err}}(\mathbf{q})\, F_{\mathrm{err}}(\mathbf{q}')\}. \tag{14}$$

For the case where $H_r = H_{\mathrm{rinv}} = H^{-1}$ and where the noise V' is uncorrelated with F_d and with itself, P_{err} is diagonal with elements $P_{\mathrm{err}}(\mathbf{q},\mathbf{q}) = V_{\mathrm{es}}(\mathbf{q})$.

The discrete-variable imaging model we have developed from the k-trajectory formulation is entirely consistent with the view of NMR imaging as a linear estimation process: Note that in Eq. (7), F_0 represents a linear observation of F_d, and in Eq. (11), F_e represents a linear estimate of F_d based on the linear observation F_0. If the additive noise is Gaussian, image formation is described as completely as possible by the means and variances of the frequency-domain components for which Eqs. (9) and (10), or (12) and (13), give approximate values.

D. Encoding procedures and imaging performance

The sampling requirements stated above are met by a very large number of generalized Fourier NMR imaging methods (all those which sample the k plane over the proper range and at the proper spacing for the object size and digital image dimension.) Although the encoding procedure for each of these methods is adequate in this sense, the details of the encoding procedure can influence the information content of the images, so that imaging performance varies a great deal among them. Here we consider in detail the influence of encoding procedure on imaging performance.

Brunner and Ernst[28] have applied to a large number of NMR imaging methods two theoretical measures of performance which appear useful in comparing the methods. These are (1) sensitivity and (2) performance time.

In terms of k-domain sampling, minimum performance time is simply determined by the number of FIDs required to adequately sample the k domain and the time devoted to each FID (often determined in practice by the relaxation times[28] T_1 and T_2). It represents the minimum data acquisition period required to acquire a complete set of data for an image, and should be an important quantity in determining the practicality of an imaging method in clinical applications (see Sec. III D).

Sensitivity is a performance index reflecting the image signal-to-noise ratio obtainable in unit time. This should be of use in judging the relative efficiency of imaging methods. Assume two imaging methods have been applied to the task of imaging the same object, using the same imaging hardware, and the minimum performance time requirement has been met for both methods. As signal averaging continues, the more sensitive method should produce an image with superior signal-to-noise ratio at any given time.

Unfortunately, the signal-to-noise ratio used in this definition of sensitivity represents signal-to-noise integrated over all spatial frequencies, and is consequently somewhat inappropriate as a measure of image quality. For example, consider the images of Figs. 2(a) and 2(b). The image in Fig. 2(b) has had its integrated signal-to-noise ratio improved by matched filtering[20] of the simulated noisy FIDs used to generate it, and as a consequence both the high spatial-frequency noise and image details have been greatly attenuated. The unfiltered image contains visual details lost in the filtered image, because the matched filter cannot judge the **adequacy** of signal-to-noise ratios in each spatial-frequency component. It simply preferentially attenuates the components expected to have lower signal-to-noise ratios, even if those signal-to-noise ratios are adequate to convey meaningful information to the observer [as they are in the case of Fig. 2(a)]. Barrett and Swindell[29] point out that the stratagem of the matched filter is appropriate for optimal *detection* (as of spectroscopic lines), but not for optimal *estimation* (as of image components).

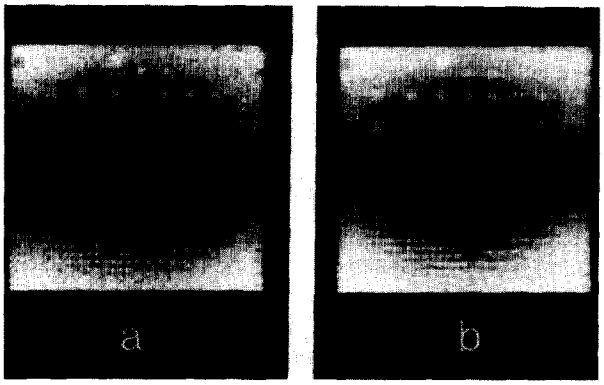

FIG. 2. (a) Simulated spin-warp image, inverse filtered, of computed phantom (see Fig. 10). (b) Simulated spin-warp image, with "matched filtering" (multiplication of FID by $\exp[-t/T_2]$). Sensitivity, in terms of total signal-to-noise ratio, is improved in Fig. 2(b). Due to loss of high-frequency information, however, visual quality of image is degraded.

An imaging method which produced the image in Fig. 2(a) would be judged by this definition of sensitivity to have poorer sensitivity than the method which produced Fig. 2(b), despite the fact that Fig. 2(b) contains demonstrably less useful information than Fig. 2(a).

Sensitivity as defined by Brunner and Ernst, then, is of limited value in comparing imaging techniques, especially when the techniques have significantly different transfer functions. More detailed and potentially more useful measures of image quality and imaging performance are available in the discrete spatial-frequency estimation means and variances of Eqs. (9)–(13).

Let us restrict our attention for now to those methods which satisfy the above sampling requirements and also sample in a rectangular or in a nearly rectangular array, so that interpolation is not necessary. For these methods the line segments over which $F(\mathbf{k})$ is sampled correspond directly to discrete spatial-frequency coordinates $\mathbf{q}$ (see Fig. 3).

In general, k trajectories may have vector time derivatives $dk(t)/dt$ which vary in magnitude and direction. In other words, the k trajectory may describe a path in $[k(t), t]$ space with curves in its projection on the k space, and its slope with respect to k space may also change arbitrarily (see Fig. 4).

If the rate of scan varies during the FID, the method's relative sensitivity and relative accuracy with respect to different spatial frequencies will vary accordingly. To see why this is so, consider the transfer function $H(\mathbf{q})$ of Eqs. (7) and (8), and consider a k trajectory which scans parallel to a coordinate axis. In this special situation (which occurs frequently in practice—see Sec. III),

$$H(q) = A\Delta t_q \exp(-t_q/T_2), \tag{15}$$

where q is a scalar ($q = 0,1,\ldots,Q$).

The relative sensitivity of the method to the qth frequency component is given by [see Eq. (11)]

$$H_r(q)\,H(q) = A\Delta t_q \exp(-t_q/T_2)\,H_r(q). \tag{16}$$

The square estimate error from Eq. (13) can be written for this one-dimensional case as

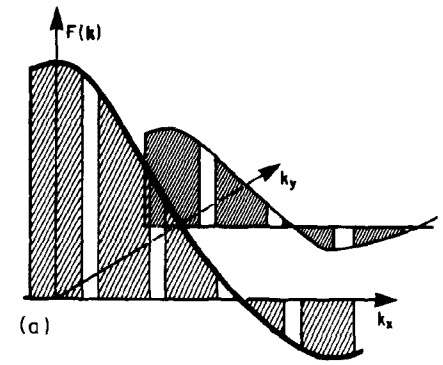

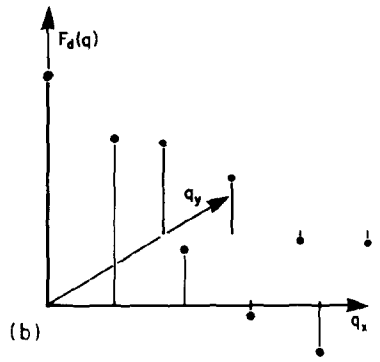

FIG. 3. The discrete spatial-frequency distribution $F_d(\mathbf{q})$ corresponds to samples of the continuous-variable distribution $F(\mathbf{k})$. For methods in which the k plane is scanned parallel to the $k_{x\ \text{axis}}$, sampling is impulsive in k_y and integrated in rectangular segments in k_x, as indicated here by the shaded areas.

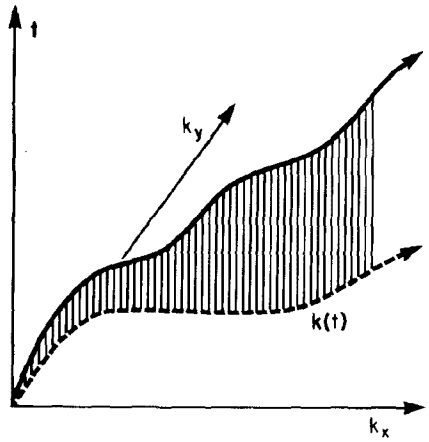

FIG. 4. An arbitrary k trajectory passing above the spatial-frequency (k) plane, with sampling path on the k plane indicated by the dashed line. At time t, the complex FID $s(t)$ is a sample of the k-domain distribution $F(\mathbf{k})$ at $\mathbf{k}(t)$, but weighted by the exponential decay $\exp(-t/T_2)$. Where $d\,|\,k(t)\,|/dt$ (equivalently, the gradient magnitude) is small, the trajectory "rises" at a more rapid rate, devoting a larger segment in time to sampling the corresponding segment of k space, thereby sampling that k location more accurately.

$$E\{|F_{err}(q)|^2\} = |[1 - H_r(q)H(q)]F_d(q)|^2 + |H_r(q)|^2 \operatorname{var}\{V'(q)\}, \quad (17)$$

where it will be recalled that $\operatorname{var}\{V'(q)\}$ is proportional to the integration time Δt_q.

This one-dimensional analysis can be extended easily to two- or three-dimensional cases where the sampling grid is rectangular (Sec. III C).

There are two types of generalized Fourier methods in which the sampling grid is not rectangular. Some rapid imaging methods (e.g., variations of the echo-planar method) sample on oblique raster lines or on sinusoidal tracks in the k plane, and hence require interpolation before Fourier inversion can be applied properly. The influence of sampling sensitivity on image quality will depend in this case on the adequacy of the sampling pattern itself.

The reconstruction from projections methods sample the k plane along radial lines. Suppose these radial lines are spaced evenly through all angles. So long as we do not attempt to reconstruct the image with azimuthal spatial frequencies beyond the limits of the data (i.e., beyond that supported by the number of projections), a reconstruction algorithm in theory can determine uniquely the original continuous (band-limited) distribution.[23]

The effects of varying sampling sensitivity in these methods are seen more easily if the functions are expressed in cylindrical expansions. Instead of grouping the sample data along radial lines as they are acquired, consider them grouped into annuli in the k plane. It has been shown[23,30] that reconstructing from projections is equivalent to estimating the coefficients in a one-dimensional harmonic expansion around each such annulus in turn, then assembling all the harmonic expansions and transforming to obtain the desired reconstructed image.

Viewed in this way, the radially decreasing system function of NMR reconstruction from projections imaging acts to decrease the accuracy of representation for those image components with higher radial spatial frequencies. We will not pursue this further, but note that it should be possible to compare directly the spatial frequency performance of reconstruction from projections methods with that of rectangular sampling grid methods by transforming (perhaps with some difficulty) between the Cartesian Fourier expansion and the cylindrical expansions used by Crowther *et al.*[30]

III. GENERALIZED FOURIER NMR IMAGING METHODS

A. Effective transfer functions

The last section presented a general description of the generalized Fourier NMR imaging methods. In this section, we discuss specific imaging techniques, including several of the established methods and several proposed methods. (The effective transfer functions for these methods are presented in Table I.) We will consider the two-dimensional case for simplicity.

To discuss the specifics of spatial-frequency performance for different NMR imaging methods, we must define the details of the timing of the gradient and sampling intervals within the FID. The time intervals involved are indicated schematically in Fig. 5.

TABLE I. Parameters of approximate discrete transfer functions for generalized Fourier NMR imaging methods.

k_f = highest k-value sampled
q_x, q_y = discrete spatial-frequency coordinates
N = dimension of (square) sampling array
T_d = delay for "ring-down" period
G_x, G_y = constant x- and y-gradient magnitudes
$\{T_y\}$ = fixed duration of phase-encoding y gradient

$H(q) = A\,\Delta t_q \exp(-t_q/T_2)$

Method	t_d	Δt_q
Original Fourier[a]	$(q_x/G_x + q_y/G_y)k_f/N$	$(T - T_d - q_y/G_y)/N$
Spin warp	$\{T_y\} + T_d + (q_x/G_x)k_f/N$	$(T - T_d - \{T_y\})/N$
R.F.P.	$[q_x^2 + q_y^2]^{1/2}k_f/GN$	$(T - T_d)/N$
Rectilinear, echo planar	$[q_x + N(q_y - 1)]T/N$	T/N, q_y even
	$[(N - q_x) + N(q_y - 1)]T/N$	T/N, q_y odd

[a] The form for rotating-frame zeugmatography[13] is essentially similar; see the text.

The period immediately following the excitation pulse is not usually available for sampling the FID signal, since the pulse itself may leave a decaying but significant signal in the receiver coil (Fig. 5). Following this "ring-down" period, the reconstruction from projections method begins sampling immediately, but most other methods must postpone sampling until after preliminary gradient phase-encoding periods, thus sacrificing a portion ($T_0 = T_y + T_d$) of the FID and losing sensitivity.

For the original Fourier method, the duration of the phase-encoding period is variable, since a constant gradient is used to drive the k trajectory to various k_x values.

In the spin-warp method, phase-encoding duration is constant for all FIDs; the amplitude of the gradient pulse is

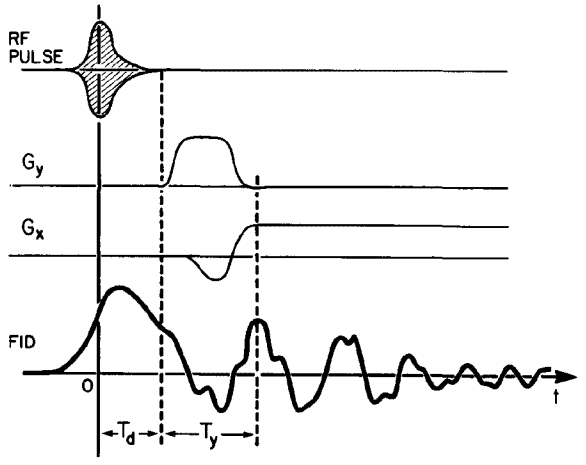

FIG. 5. Timing relationships during a single FID of a simplified spin-warp method in which selective irradiation for plane selection is not used. G_x and G_y denote the x and y gradients, respectively; the pulsed G_y accomplishes phase encoding. A preliminary ring-down period T_d and phase-encoding period T_y precede the period devoted to FID sampling, which extends to a time T.

altered rather than its duration. Constant-duration phase encoding reduces the adverse effects of field inhomogeneity on the image.[6]

For the single-FID methods, which do not require phase encoding, the k-plane scan begins immediately following the ring-down period.

The "rotating-frame" methods of Hoult[13] accomplish phase-encoding by means of radio-frequency gradients rather than static field gradients, but a similar variable period prior to data acquisition must be devoted to phase encoding in this case as well.

Figure 6 depicts typical k trajectories for these methods and others. The relative two-dimensional transfer functions and error variance functions which result are shown graphically in Fig. 7 for a common set of conditions.

There are many types of restoration and enhancement filters which could be used in NMR imaging. The most commonly used filtering methods correspond to discrete convolution in the spatial domain: i.e., they are linear and shift invariant, so that such discrete filters can always be represented exactly by a frequency-domain response function $H_r(\mathbf{q})$. The inverse filter assures that the final frequency-domain image $F_e(\mathbf{q})$ will be unbiased; i.e., the value expected for each of the q components is the actual value of that component. For faithful rendition of the original object, the inverse filter is the ideal filter in the noise-free limit. As the amount of noise in the input data is increased, the signal-to-noise ratios of the higher spatial frequencies are generally the first to become unacceptably low. In order to suppress the higher spatial frequencies now dominated by noise, a low-pass filter is usually used.

In NMR imaging, as in imaging by typical optical systems, transfer functions $H(\mathbf{q})$ tend to attenuate high spatial frequencies more than low frequencies. The unfiltered image $F_0(\mathbf{q})$, then, has under-represented high frequencies and a level noise distribution $V(\mathbf{q})$. Thus at progressively larger values of $|\mathbf{q}|$, the signal-to-noise ratios tend to decrease until $F_0(\mathbf{q})$ has an unacceptably large error variance. Nothing is gained by representing these components in the final image—they are dominated by noise.

A common strategy of linear enhancement filtering,[26,27] then, is to restore those components attenuated by $H(\mathbf{q})$ but which retain adequate signal-to-noise ratios, and to attenuate strongly those higher frequency components with insufficient signal-to-noise ratios. This type of filter is in effect a combined low-pass and inverse filter.

If a fixed amount of time is available in which to image by one of the generalized Fourier NMR imaging methods, that time must be devoted to sampling an appropriate range of spatial frequencies at an appropriate sampling density, as we saw in Sec. I. Within this fixed period, each discrete spatial frequency has its own effective signal-averaging time, and as we suggested earlier, the allocation of sampling time among the spatial frequencies determines the relative accuracy with which the spatial-frequency components are measured. Thus by altering gradients and sampling rates appropriately, one can control the functional dependence of both $H(\mathbf{q})$ and $V_{es}(\mathbf{q})$.

The potential value of this control in NMR imaging is that

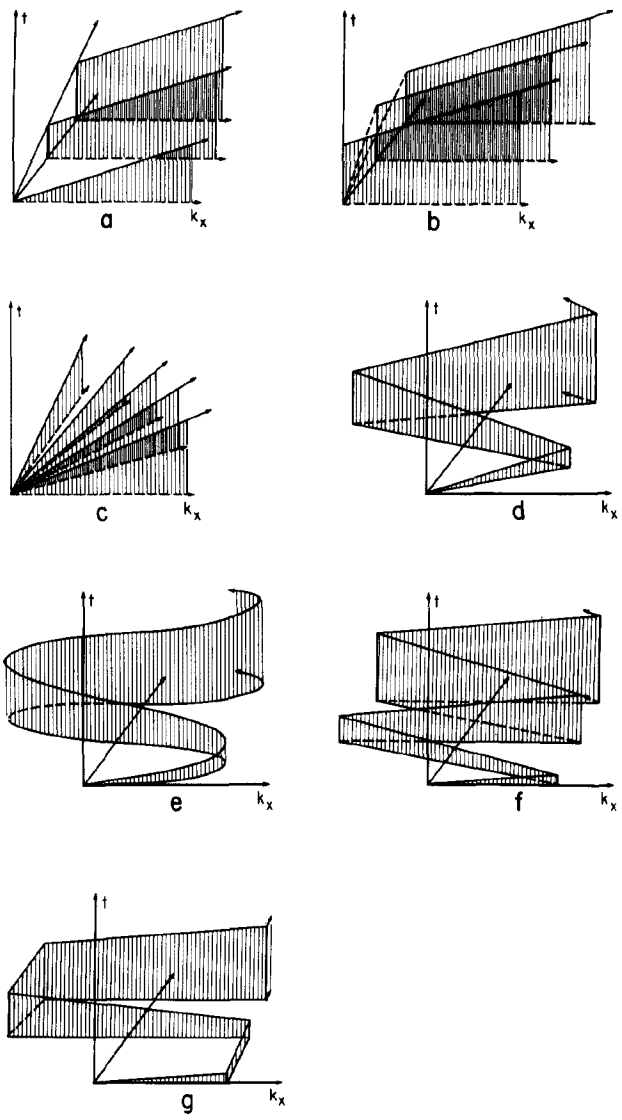

FIG. 6. k trajectories for several NMR imaging methods: (a) the original Fourier method (Ref. 5), (b) the spin-warp method (Ref. 6), (c) the reconstruction from projections method (Refs. 7 and 9), (d) the echo-planar method (Refs. 10–12), (e) a sinusoidal modification of the echo-planar method (Ref. 14), (f) the method of Creyghton *et al.* (Ref. 16), and (g) a proposed rectilinear scanning method. The last four methods may be used to produce a complete image (without regard to signal-to-noise considerations) during a single FID.

in effect, a greater amount of useful information regarding the object can be placed into the data per unit time than is possible when constant gradients and uniform sampling periods are used.

Allocation of signal-averaging time among spatial frequencies is most easily accomplished among the spatial frequencies located along a single FID—on a single k trajectory. For methods which use multiple FIDs, allocation of signal-averaging time among components occurring on separate FIDs must be accomplished, in general, by repeatedly sampling the same locations. For single-FID methods, the

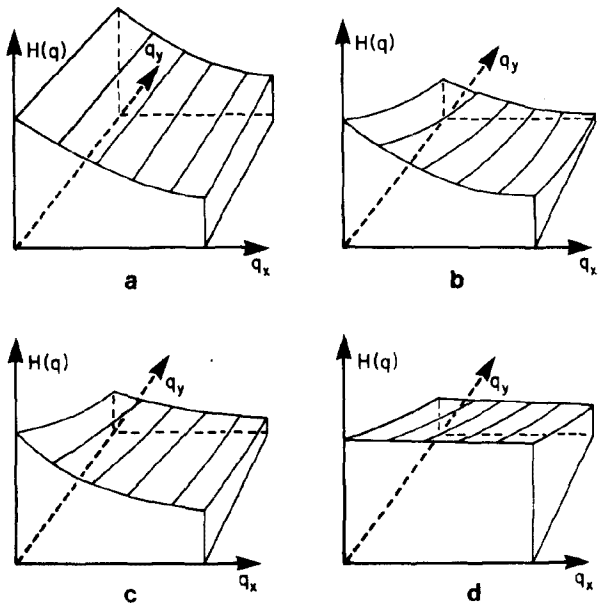

FIG. 7. Schematic depictions of transfer functions $H(q)$, demonstrating spatial-frequency sensitivity of several methods: (a) the spin-warp method [Fig. 6(b)], (b) the original Fourier method [Fig. 6(a)], (c) the reconstruction from projections methods, and (d) the single-FID techniques, in which the k plane is scanned slowly in the k_y direction and rapidly in the k_x direction. In methods for which negative q_x values are sampled, $H(q_x, q_y) = H(-q_x, q_y)$.

entire k plane is sampled by a single k trajectory, so that choosing Δt_q and t_q for all q is a straightforward matter.

As indicated by Eq. (15) and Fig. 7, the high-frequency insensitivity of those generalized Fourier methods with constant gradients is dependent on the duration of the sampling time $(T - T_0)$ relative to the transverse relaxation time T_2. If the sampling time is short with respect to T_2, the domination of the transfer function by low frequencies, and the concomitant imaging performance problems, might seem to be eliminated. However, as sampling times $(T - T_0)$ become briefer, the effective signal-averaging time and signal-to-noise ratio are reduced for all components. Thus, even for lower frequencies, methods using longer sampling times (e.g., $T = 2T_2$) and nonlinear k trajectories to achieve improved spatial-frequency response retain a theoretical performance advantage over constant gradient, brief acquisition methods. [Equations (22) and (23) can be used to show that at $k = 0$, sampling time with constant gradient must exceed $T_2/2$ to equal the accuracy of the equal error variance (EEV) method with $2T_2$ sampling time.]

B. Echoes

In all cases, it simplifies data processing to have the k trajectory crossing one of the k axes at the beginning of the sampling. This is accomplished by a preliminary "dephasing" gradient pulse[6] which produces an echo in the FID signal at the beginning of sampling.

Complete sampling of the pertinent regions of the k plane demands that low spatial frequencies near the k axes and the origin be sampled; eliciting echoes either at the beginning of the sampling period[6] or during the sampling period[11,12] can help accomplish this. Sampling directly at the origin of k space is not possible with a constant gradient which is begun before the rf pulse, a usual arrangement in the reconstruction from projections method.[7]

Echo planar methods[10–12] and similar methods[14–16] likewise use echoes during a single FID which scans the required portion of the k plane. In this case, the echoes are elicited repeatedly (either by reversing gradients or by applying 180° pulses) as the k trajectory recrosses the k_y axis at successively larger values of k_y, as seen in Fig. 8.

It is not true that eliciting echoes enhances imaging sensitivity. The echo signal simply corresponds to the local maximum in $|F[\mathbf{k}]|$ which occurs at $k_x = 0$ for fixed k_y because $f(\mathbf{x})$ is real and positive. The same total acquisition time must still be apportioned somehow among the spatial-frequency components.

C. The equal error variance method

Under many (if not most) circumstances, an unbiased image would be desirable. This type of image would correspond most closely, in the mean, to the original distribution. Thus imaging methods are of interest which use inverse filters $Hr_{\text{inv}}(\mathbf{q})$ in conjunction with whatever the imaging transfer function $H(\mathbf{q})$ might be.

As was shown in Sec. II, the error variance function $V_{\text{es}}(\mathbf{q})$ and expected error bias can be simultaneously specified, so that there exists in theory an unbiased imaging method with any shape error variance function we desire.

One unbiased method of particular interest is the equal error variance method, which has equal rms error expected for each frequency component. This seems to offer an improvement over the conventional methods, in which error variance increases with frequency while the expected magnitude of the frequency components (for typical images) decreases in general with frequency.

For this method, the unbiased estimate error variance [the second term on the right-hand side of Eq. (17)] is constant for all q. Thus,

$$|H_r(q)|^2 \operatorname{var}\{V'(q)\} = C, \tag{18}$$

where C is a constant, for all q. Because the method is unbi-

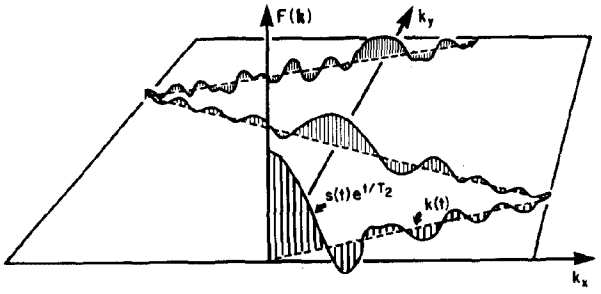

FIG. 8. Echo production viewed as the return of the k trajectory across the k_y axis, where the magnitude of the Fourier-domain object distribution $F(\mathbf{k})$—and hence the signal $s(t)$—reach a local maximum. The sawtooth k trajectory shown is that of the echo-planar method [see Fig. 6(d)].

ased, $Hr(q) = 1/H(q)$, where $H(q)$ is given by Eq. (15). Since var $\{V'(q)\}$ is just $\sigma_q^2 \Delta t_q$ (where σ_q^2 is the unweighted noise variance of the qth component), we then have

$$\sigma_q^2 \Delta t_q / [A^2 \Delta t_q^2 \exp(-2t_q/T_2)] = C \tag{19}$$

or for noise stationary in q,

$$A^{-2} \Delta t_q^{-1} \exp(2t_q/T_2) = C', \tag{20}$$

where C' has absorbed the constant σ (note the equal error variance solution will be different for correlated or nonstationary noise). The method we seek uses a gradient which is a continuous function of time, so we consider the limiting case of small increments Δt, and obtain

$$dk(t)/dt = C'' \exp(-2t/T_2) \tag{21}$$

for the condition on the k trajectory corresponding to equal error variance. Since the gradient field is proportional to dk/dt, this result gives the form of the necessary gradient time dependence directly. Although Eq. (21) describes a scalar function $k(t)$, it applies directly to two- and three-dimensional cases as well if the vector magnitude $|\mathbf{k}(t)|$ is used in place of $k(t)$.

Figure 9 is a plot of the k_x dependence of the estimate error variance computed for the spin-warp method and the EEV modification of the spin-warp method. Note that in absolute terms, the EEV image errors will be larger for lower frequencies than the spin-warp errors, but that EEV errors will be smaller at higher frequencies. Thus, unneeded accuracy at low frequencies is traded for desired accuracy at higher frequencies.

This can be demonstrated quantitatively by considering the k_x dependence of the error variance (which is constant in k_y for the spin-warp and EEV/spin-warp methods). From Eq. (17) it can be shown that in the continuous-variable limit (as $Q \rightarrow \infty$), spin-warp error variance becomes

$$V_{es}(k) = A^{-2}\sigma^2 \frac{k_f}{T} \exp[2kT/k_f T_2], \tag{22}$$

and the EEV error variance becomes

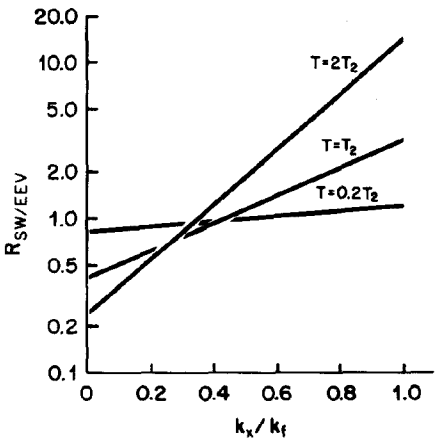

FIG. 9. Ratio $R_{SW/EEV}$ of estimate error variance of the spin-warp method to that of the EEV method, plotted logarithmically as a function of k_x (the ratio is constant in k_y). The longer the sampling period T extends relative to T_2, the more marked becomes the advantage in high spatial frequency accuracy of the EEV method.

$$V_{es}(k) = A^{-2}\sigma^2 \frac{2k_f}{T_2} [1 - \exp(-2T/T_2)]^{-1}. \tag{23}$$

The ratio of the spin-warp to EEV error variances is

$$R_{sw/EEV} = \frac{T_2}{2T} [1 - \exp(-2T/T_2)] \exp(2kT/k_f T_2), \tag{24}$$

which is plotted in Fig. 9 for $T/T_2 = 0.2$, 1, and 2. It can be shown that the ratio of integrated error variances is just

$$\int V_{es}^{sw}\, dk \Big/ \int V_{es}^{EEV}\, dk = \left[\sinh\left(\frac{T}{T_2}\right) \Big/ \left(\frac{T}{T_2}\right)\right]^2. \tag{25}$$

For the (T/T_2) values of 0.2, 1, and 2, the ratio (spin warp to EEV) of integrated error variances is 1.013, 1.381, and 3.289, respectively, indicating the performance advantage of the EEV method becomes more appreciable for FID acquisition times T long with respect to T_2.

Figure 10 presents the results of preliminary simulation studies including the tracking bandwidth and constant bandwidth implementations of the EEV method, along with the spin-warp method unfiltered, inverse filtered, and Wiener filtered. The Wiener[26,27,29] filter represents a combination inverse and low-pass filter which takes into account several pieces of *a priori* information: the system transfer function H, the noise power spectrum, and the object power spectrum. The last is not likely to be available in practice, since the object distribution is usually assumed entirely unknown, so that the Wiener filter could not perform in practice as well as it does here, supplied with the correct object spectrum. The Wiener filtered image is intended to represent the "best" image one could reasonably expect from the spin-warp method under the conditions of this simulation, and is included only for purposes of comparison.

Note that low-contrast details are more readily discernible in the EEV images than in the spin-warp image, indicating that the increased information (i.e., reduced uncertainty) in the higher spatial frequencies indeed has a visually significant effect.

The EEV method serves as a useful example in discussing some of the technical problems to be anticipated in methods with time-varying gradients. One of these is noise bandwidth. Because the gradient for the EEV method decreases exponentially in time, the bandwidth occupied by the useful image data decreases exponentially in time as well. Clearly, if the spin-warp method and the EEV method both acquire FID data until $2T_2$ has elapsed, they will have reached the same point in k space at the time $2T_2$. In doing so, however, the EEV gradient will begin at a higher value than the constant spin-warp gradient, but will end at a lower value. Since the signal bandwidth is proportional to the gradient, the signal bandwidth will begin with a large value and decrease to a small value. To minimize the noise introduced into the digitized FID, then, the bandwidth of the analog filter preceding the ADCs should track the signal bandwidth throughout the FID. Unfortunately, special purpose hardware to accomplish this may not be readily available, so that one must use a constant bandwidth filter set at the maximum required signal bandwidth of the EEV method, which occurs at the be-

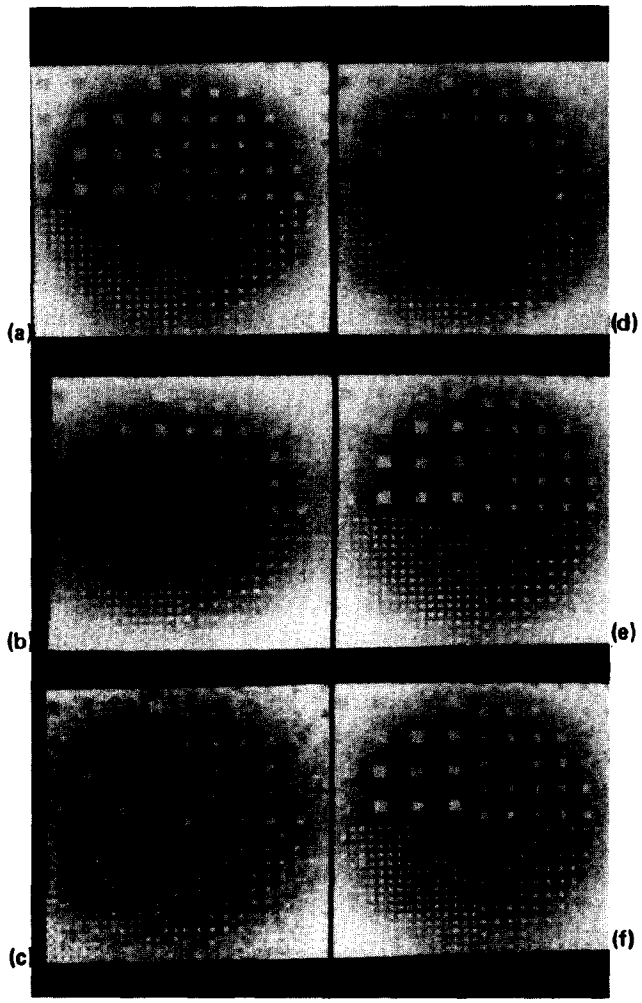

FIG. 10. Simulated 64×64 NMR images demonstrating contrast and noise level differences in standard spin-warp and EEV modified methods: (a) phantom image with no noise. Small squares have constant level; background increases radially from center. (b) Spin warp with no filtering, (c) spin warp with inverse filter, (d) spin warp with Wiener filter, (e) EEV with bandwidth tracking, and (f) EEV with constant bandwidth. Noise was uncorrelated and Gaussian, and data acquisition period $T = 2T_2$ in all cases. Simulation was performed using Perkin–Elmer 3220 computer with Genisco display system.

ginning of the FID.

In both the tracking bandwidth and the constant bandwidth implementations of the EEV method, high-frequency representation accuracy is theoretically superior to that of the conventional methods which use constant gradients and uniform sampling intervals [see Eq. (24) and Fig. 9].

The nonuniform sampling intervals made necessary by the changing k trajectory scanning rate also require special attention. In practice, the nonuniform sampling intervals may be realized by sampling at a higher rate than would be required normally, then recombining the samples over varying time intervals so that the k interval sampled is relatively constant. Multiplication of each composite datum by an appropriate fixed factor would compensate for errors due to discretization of the time intervals.

D. The single-FID methods

In some applications of NMR imaging, it is important—even essential—to form an image in the briefest possible period.[11,12] Among the reasons for this are (1) to minimize the effects of organ motion, and (2) to increase the number of imaging studies that can be done within a given length of time.

Largely because of these considerations, imaging methods have been developed[11–16] which allow a reduction in minimum performance time by scanning the k plane during a single FID.

Just as k trajectories may be used which traverse the k plane at variable rates, so k trajectories may also describe any of an infinite number of possible sampling pathways on the k plane which satisfy the basic sampling requirements. Single-FID pathways satisfying these requirements could describe spirals, or curvilinear, rectilinear, or sawtooth raster patterns on the k plane (see Fig. 6). Individually, the advantages and disadvantages of these will be in terms of the practical difficulties in driving rapidly changing gradient waveforms and in the complexity of processing (decoding) the data.

Although the data processing necessary for image formation may be simpler for sawtooth and rectilinear k trajectories, the gradient-driving hardware must sustain larger high-frequency components. For the curvilinear k trajectories, on the other hand, technical difficulties in implementation will tend to be computational rather than instrumental, since these methods should have additional interpolation computations prior to Fourier inversion for best results. Although images can be produced from the sawtooth scan of the echo-planar method without benefit of interpolation, image quality may be somewhat degraded thereby. The method of Creyghton *et al.*[16] [Fig. 6(f)], when odd-numbered echoes are ignored, samples on a rectangular grid, so it is not necessary to interpolate to avoid image distortion. By using 180° pulses to reverse the k trajectory, large-magnitude switched gradients are avoided.

Alternative methods scanning the k domain in a rectilinear fashion may have some advantages. The method of Fig. 6(g), for instance, would allow somewhat more efficient use of the time available for sampling.

When these methods are implemented in such a way as to acquire all data within a period much shorter than T_2 (as might be desirable in gated cardiac imaging, for instance), the transfer function is essentially uniform in frequency though sensitivity for each frequency is reduced. Thus in the inverse-filtered implementation, these methods will have approximately the unbiased and equal error variance properties discussed above, even if the gradient magnitude is constant while the FID is sampled.

When one of these methods scans the k plane in a time comparable to T_2, however, the transfer function will decrease exponentially along the track of the k trajectory—it will have approximately the shape of the transfer function for the spin-warp method. Thus neglecting effects of nonuniform sampling (which occurs for the curvilinear and sawtooth-type k trajectories), the performance characteristics will be nearly the same as for the spin-warp method.

E. Imaging methods which are "optimal estimators"

Another group of generalized Fourier NMR imaging methods of particular interest are the methods which correspond to optimal estimators of the distribution $F_d(\mathbf{q})$.

NMR imaging is an estimation process in the sense that one would like the final image to be a good estimate of the continuous distribution $f(x)$. The term estimate is used here to indicate that the image should match the object in some precisely defined sense, and also because the relationships we have observed between the image distribution and the object distributions in the spatial-frequency domain are identical to those of the classical linear estimation problem. This correspondence between NMR imaging and the estimation problem implies that useful results of estimation theory may be applied directly to the problem of NMR imaging.

Through Eqs. (16) and (17), the net relative sensitivity and accuracy of an imaging method's spatial-frequency response can be determined from its k trajectories and its sampling scheme. Moreover, we can now derive new imaging methods with desired spatial-frequency characteristics.

Specifically, by choosing the sampling sequence t_q $(q = 0,1,...,N-1)$ during the available acquisition period of the FID, and by selecting the restoration filter coefficients $H_r(q)$, we can choose in effect the net transfer function (or alternatively, the error bias) via Eq. (16), and the net estimation error variance profile via Eq. (17).

Optimal image processing techniques have often been used in biomedical imaging applications.[29,32,33] Optimal NMR imaging, however, implies something more than optimal processing of already existing digital images. In NMR imaging, the data acquisition process itself may be designed to preferentially gather the information of most importance. Thus in an optimal NMR imaging method, both the processing and the encoding are optimal.

As a result, there is more to be gained in terms of performance by using optimal NMR imaging methods than can be gained in other medical imaging methods by optimal image processing alone.

There are two categories of optimality criteria we might seek to maximize in NMR imaging. We could look for the imaging method which achieves the best image quality in terms of some statistical measure such as least-square error. On the other hand, we could look for the method which will produce images with the best diagnostic "readability," based on some model of the visual diagnostic interpretation process, perhaps specific to a given diagnostic task (such as the "Rose model" [34] applied to detection of low-contrast lesions).

Established techniques of optimal estimation[31] and optimization[35] may also allow us to determine optimal methods for cases in which noise is correlated with itself or with the object, and in which system constraints are considered (for instance, when gradient fields or their rates of change must be limited in range due to hardware restrictions). In theory, the k-trajectory formulation permits one to derive an imaging method optimal with respect to any performance criterion expressible in k-domain terms, while considering effects of practical matters such as hardware imposed or software imposed constraints, or *a priori* knowledge of the noise power spectrum or the object distributions to be expected.

There is, of course, no guarantee that for a given set of design specifications (i.e., optimality criterion, constraints, and *a priori* knowledge of noise and object distribution) the resulting optimal method will perform substantially better than one of the conventional nonoptimal methods, but the apparent performance advantages of the EEV method suggest that in many cases it will.

The equal error variance method is a simple example of an optimal method; it can be shown that the EEV method is the unbiased estimator optimal in the minimum variance sense for uncorrelated noise.

IV. SUMMARY AND CONCLUSIONS

The purpose of this communication has been to present an alternative theoretical view of the process of NMR imaging, together with some of its applications. This model applies to most existing NMR imaging methods, as well as a large number of untried but potentially workable methods.

Whereas the conventional model of NMR imaging centers on the correspondence between the spectrum of the transient response (the FID) and projections of the unknown spatial distribution, the k-trajectory model views the FID itself as a noisy observation of the spatial-frequency distribution which is the Fourier transform of the unknown spatial distribution to be imaged. (Both views are correct, but the k-trajectory view may be more useful in some respects.)

The k trajectory is simply the path in spatial-frequency space over which the sampling process occurs, and it is completely determined by the gradient fields applied during the FID. Any k trajectory or set of k trajectories which scans an appropriate region of the spatial-frequency domain can be used to produce an image. The rapid imaging methods can form an image from data acquired during a single FID, using a single k trajectory to scan the spatial-frequency domain.

Although it gives an intuitively useful graphic depiction of the imaging process, the major potential value of the k-trajectory model lies in its ability to account quantitatively for the influence of relaxation times, time-varying gradients, and FID sampling schemes on image quality. Not only does this permit analysis of theoretical imaging performance for existing methods, but it also permits prediction of imaging performance for proposed imaging methods with arbitrary time-varying gradients and FID sampling schemes. This latter property in turn allows synthesis of new imaging methods with specified imaging performance characteristics.

In generalized Fourier methods optimal for a given performance criterion, performance may be significantly better than in existing imaging methods. This is true especially for performance criteria in which accuracy of higher spatial-frequency rendition is important, since most existing methods overemphasize accuracy of low-frequency rendition at the cost of accuracy in the higher frequencies.

Note that image processing can alter the magnitude of various image spatial frequencies, but not the accuracy with which they are represented. This relative accuracy is determined in generalized Fourier NMR imaging by the time dependence of the applied gradient fields. That is, once image

data has been acquired, we cannot improve its information content, no matter what processing method we try. But by manipulating gradients judiciously, and keeping track of where in the k domain we are sampling at each moment, we may preferentially acquire the image information of most concern.

Perhaps the most meaningful measures of imaging performance for biomedical applications are based on models of visual interpretation, rather than on purely statistical considerations. Short of this, an intuitively reasonable performance specification would be equally accurate representation of all spatial frequencies, rather than the bias in accuracy (i.e., information) toward the lower spatial frequencies exhibited by most existing NMR imaging methods.

This latter requirement can be achieved readily in NMR imaging, simply by using exponentially decaying gradient fields, and an appropriate FID sampling schedule, as we have shown in the discussion of the EEV methods. Comparisons of simulated NMR images seem to verify visual contrast and rendition of details are significantly better in the EEV images than in unfiltered or optimally filtered "conventional" (constant gradient) NMR images.

The k-trajectory description and the techniques of analysis and synthesis to which it gives rise are general. They can be applied to imaging methods which use any type of plane selection, multiple-pulse sequences (for relaxation time imaging), in two- or three-dimensional applications, and in single-FID rapid imaging implementation or multiple-FID implementations.

At least for the simpler examples of derived generalized Fourier NMR imaging methods, implementation will not place great additional demands on gradient hardware or data handling software. In fact, some existing instruments should be capable of imaging with these methods with minor software modifications alone.

The k-trajectory formulation and the linear discrete imaging model developed here appear to provide powerful but practical tools for analyzing the theoretical performance of NMR imaging methods in detail, and for designing new NMR imaging methods with optimal performance in any desired sense and in the presence of instrumental and other technical constraints.

ACKNOWLEDGMENTS

I would like to acknowledge the assistance of Ms. Gayle Blust in the preparation of the manuscript, and Ms. Dorothy Gutekunst for photographic assistance. This work was supported in part by NIH Ischemic Heart SCOR (HL-17669), and in part by the American Heart Association Texas Affiliate.

[1]T. R. Brown, B. M. Kincaid, and K. Ugurbil, Proc. Natl. Acad. Sci. U.S.A. **79**, 3523 (1982).
[2]D. B. Twieg, Proc. Soc. Photo-Opt. Instrum. Eng. **347**, 354 (1982).
[3]P. Mansfield and P. G. Morris, *NMR Imaging in Biomedicine* (Academic, New York, 1982), Chap. 3.
[4]W. S. Hinshaw, J. Appl. Phys. **47**, 3709 (1976).
[5]A. Kumar, D. Welti, and R. Ernst, J. Magn. Reson. **18**, 69 (1975).
[6]W. Edelstein, J. Hutchison, G. Johnson, and T. Redpath, Phys. Med. Biol. **25**, 751 (1980).
[7]P. C. Lauterbur, Nature **242**, 190 (1973).
[8]C.-M. Lai and P. C. Lauterbur, Phys. Med. Biol. **26**, 851 (1981).
[9]C.-M. Lai and P. C. Lauterbur, J. Phys. E **13**, 747 (1980).
[10]P. Mansfield, J. Phys. C. **10**, L55 (1977).
[11]P. Mansfield and I. Pykett, J. Magn. Reson. **29**, 355 (1978).
[12]R. Ordidge, P. Mansfield, and R. Coupland, Br. J. Radiol. **54**, 850 (1981).
[13]D. I. Hoult, J. Magn. Reson. **33**, 183 (1979).
[14]M. M. Tropper, J. Magn. Reson. **42**, 193 (1981).
[15]H. B. Song, Z. H. Cho, and S. K. Hilal, IEEE Trans. Nucl. Sci. **29**, 493 (1982).
[16]J. H. N. Creyghton, M. J. Duijvestijn, J. v. Eggermond, J. Smidt, and R. A. Wind, J. Magn. Reson. Med. (to be published).
[17]D. G. Taylor, D. May, and M. C. Jones, Phys. Med. Biol. **26**, 931 (1981).
[18]R. J. Sutherland and J. M. S. Hutchison, J. Phys. E **11**, 79 (1978).
[19]H. R. Brooker and W. S. Hinshaw, J. Magn. Reson. **30**, 129 (1978).
[20]R. R. Ernst and W. A. Anderson, Rev. Sci. Instrum. **37**, 93 (1966).
[21]D. Shaw, *Fourier Transform NMR Spectroscopy* (Elsevier, New York, 1976).
[22]A. Abragam, *The Principles of Nuclear Magnetism* (Oxford, London, 1961).
[23]A. Klug and R. Crowther, Nature (London) **238**, 435 (1972).
[24]R. Bracewell, *The Fourier Transform and Its Applications* (McGraw-Hill, New York, 1978).
[25]J. M. Libove and J. R. Singer, J. Phys. E **13**, 38 (1980).
[26]W. K. Pratt, *Digital Image Processing* (Wiley-Interscience, New York, 1978).
[27]A. Rosenfeld and A. C. Kak, *Digital Picture Processing* (Academic, New York, 1976).
[28]P. Brunner and R. R. Ernst, J. Magn. Reson. **33**, 83 (1979).
[29]H. H. Barrett and W. Swindell, *Radiological Imaging* (Academic, New York, 1981).
[30]R. A. Crowther, D. J. DeRosier, and A. Klug, Proc. R. Soc. London Ser. A **317**, 319 (1970).
[31]A. P. Sage and J. L. Melsa, *Estimation Theory with Applications to Communications and Control* (McGraw-Hill, New York, 1971).
[32]E. Tanaka and T. A. Iinuma, Phys. Med. Biol. **15**, 683 (1970).
[33]D. C. Barber and J. R. Mallard, Phys. Med. Biol. **16**, 635 (1971).
[34]R. F. Wagner, Med. Phys. **4**, 279 (1977).
[35]D. J. Wilde and C. S. Beightler, *Foundations of Optimization* (Prentice-Hall, Englewood Cliffs, New Jersey, 1967).